QCD analysis of Lambda hyperon production in DIS target-fragmentation region

Federico Alberto Ceccopieri[(a,b)*] and **Davide Mancusi**[(a,c)†]

[(a)] *IFPA, Université de Liège,*
Allée du 6 août, Bât B5a, 4000 Liège, Belgium

[(b)] *Université Libre de Bruxelles,*
Boulevard du Triomphe, 1050 Bruxelles, Belgium

[(c)] *CEA, Centre de Saclay, IRFU/Service de Physique Nucléaire,*
F-91191 Gif-sur-Yvette, France

Abstract

We consider Lambda-hyperon production in the target-fragmentation region of semi-inclusive deep-inelastic scattering within the framework of fracture functions. We present a first attempt to determine the flavour and energy dependences of these non-perturbative distributions through a simultaneous QCD-based fit to available neutral- and charged-current semi-inclusive-DIS cross sections. Predictions based on the resulting nucleon-to-Lambda fracture functions are in good agreement with data and observables not included in the regression. The successful prediction of the Q^2 dependence of the Lambda multiplicity notably represents the first validation of the perturbative framework implied by fracture functions.

*Email address : federico.ceccopieri@hotmail.it
†Email address : davide.mancusi@cea.fr

1 Introduction

It has been known for a long time [1] that in hadronic collisions the longitudinal momentum spectrum of particles produced in target fragmentation crucially depends on the difference of the valence-parton composition of the initial- and final-state particles. In particular, only an initial-state particle whose valence-quark flavour content is almost or totally conserved in the scattering can be a leading particle in the final state, *i.e.* carry a substantial fraction of the incoming projectile energy. Simple counting rules connect the differences in the valence-parton composition of initial- and final- state particles with the shape of longitudinal momentum spectrum of the latter. Leading particles in the final state are typically characterised by large longitudinal momentum fractions and very small transverse momenta with respect to the collision axis, a typical regime dominated by soft QCD dynamics where standard perturbative techniques cannot be applied.

The leading particle effect manifests itself in reactions involving at least one hadron in the initial state. Quite interestingly, it also appears in processes which involve point-like probes, such as Semi-Inclusive Deep Inelastic Scattering (SIDIS) and, as a special case of the latter, find spectacular realisation in diffractive DIS. At variance with other processes discussed above, such process involves a large momentum transfer which enables the use of perturbative QCD. Semi-Inclusive DIS, in fact, provides detailed information on both the partonic structure of hadrons and on the fragmentation of partons into final-state hadrons. This information is generally extracted from the so called current-fragmentation region, *i.e.* the phase-space region in which the struck parton hadronises. The target-fragmentation region is instead sensitive to the hadronisation properties of the coloured spectator system which results from the removal of one parton from the incident nucleon by the virtual probe. For these reasons, the description of particles production in this particular region of phase space through standard perturbative calculations based on parton distributions and fragmentation functions will fail when compared to data. The description can be improved only with the introduction of new non-perturbative distributions which encode these peculiar aspects of QCD dynamics.

This was early realised in Ref. [2] where the authors introduced the concept of fracture functions. These distributions simultaneously encode information about the parton interacting with the hard probe and about the fragmentation properties of the spectator system. Although intrinsically of non-perturbative nature, the scale dependence of such distributions can be calculated within perturbative QCD [2]. Fracture-functions evolution is driven by inhomogeneous Altarelli-Parisi equations which result from the structure of collinear singularities in the target-fragmentation region [2, 3]. Moreover, the factorisation theorem [4, 5] guarantees that fracture functions are universal distributions, at least in the context of SIDIS, and this fact constitutes a solid support for phenomenological analysis.

The phenomenology which makes use of all these concept is confined to the study of hard diffraction in Deep Inelastic Scattering and, to the best of our knowledge, no analysis has so far been attempted for particles other than proton in the final state. It is well known, however, that Lambda hyperon production in SIDIS on proton is mainly concentrated in the target-fragmentation region since Lambdas show a significant leading particle effect.

In this paper we describe how a variety of Lambda leptoproduction cross sections can be simultaneously described within the fracture-function approach, if these non-perturbative distributions are modelled at some low scale and if their free parameters are determined by a fit

to the available data. The rather scarce Lambda leptoproduction data in general do not allow to directly verify the leading-twist nature of this type of processes, which is implicitly assumed in the fracture-function framework, nor allow to test the scale dependence embodied by their specific evolution equations. In this respect, both the formalism and the model presented in this paper require more experimental information for a conclusive validation. We believe, however, that a quantitative tool that is able to reproduce many aspects of the existing data may further stimulate both the theoretical and the experimental activity. As a by-product, the model will give us the first insights on the flavour and energy dependences of the fragmentation properties of the spectator system into Lambda hyperons.

The paper is organized as follows. In Section 2 we briefly recall basic SIDIS cross sections and fracture-function properties. In Section 3 we discuss specific features of the data sets and observables used in the analysis. In Section 4 we describe a simple model for Lambda fracture functions and in Section 5 we provide and discuss the results of our fit. In Section 6 we compare the resulting model predictions for data and observables not used in the fit. We finally collect our conclusions in Section 7.

2 Semi-Inclusive DIS in the target-fragmentation region

The deep inelastic scattering cross section of a lepton l off a proton p with four-momenta k and P, respectively, is described in terms of the lepton variables:

$$x_B = \frac{Q^2}{2P\cdot q}, \quad y = \frac{P\cdot q}{P\cdot k} = \frac{Q^2}{s_h x_B}, \quad Q^2 = -q^2, \tag{1}$$

where k' and $q = k - k'$ are the outgoing lepton and virtual photon four-momenta, respectively, $s_h = (P+l)^2$ is the centre of mass energy squared and $W^2 = s_h y(1-x_B) + m_p^2$ is the invariant mass squared of the final state, with m_p^2 being the proton mass. The additional invariant [3]

$$z_h = \frac{P\cdot h}{P\cdot q} = \frac{E_h}{E_P(1-x_B)}\frac{1-\cos\theta_h}{2}, \tag{2}$$

is often used to specify the kinematics of final state hadron with four-momentum h, where E_h and θ_h are the detected hadron energy and angle respectively defined in the virtual photon-proton centre of mass frame. The variable z_h is however not adequate to describe target fragmentation, since both soft hadron production ($E_h \simeq 0$) and hadron production in the target-remnant direction ($\theta_h \simeq 0$) both yield a vanishing value of z_h. We therefore consider cross sections differential either in the scaled hadron energy variable z or ζ [3]

$$z = \frac{\zeta}{1-x_B}, \quad \zeta = \frac{E_h}{E_P}, \tag{3}$$

again defined in the $\gamma^* p$ centre of mass frame. The final state hadron is detected in the final state with a fraction $z \in [0,1]$ of the spectator energy $E_p(1-x_B)$. In the following we will analyse data presented in term of Feynman's variable

$$x_F = \pm\Big(z^2 - \frac{4m_T^2}{W^2}\Big)^{\frac{1}{2}}. \tag{4}$$

We adopt the convention that, in the $\gamma^* p$ frame, negative values of x_F are attributed to final state hadrons moving parallel to incoming proton direction. Hence we assume that, in the quark-parton model, the target-fragmentation region is defined by the frame-dependent condition $x_F < 0$. In eq. (4) we have introduced the hadron transverse mass, $m_T^2 = m_h^2 + p_{h,\perp}^2$, defined in terms of its transverse momentum and mass squared.

In the quark-parton model, the neutral-current semi-inclusive DIS cross section for producing an unpolarised Lambda off a proton in the target-fragmentation region reads [3]

$$\frac{d^3\sigma^{lp\to l\Lambda X}}{dx_B dQ^2 d\zeta} = \frac{2\pi\alpha_{em}^2}{Q^4} J Y_+ \sum_{q=u,d,s} e_q^2 \Big[M_q^{\Lambda/p}(x_B, Q^2, \zeta) + M_{\bar{q}}^{\Lambda/p}(x_B, Q^2, \zeta) \Big] , \tag{5}$$

where $Y_+ = 1 + (1-y)^2$. The cross section has been re-expressed for later convenience in term of the ζ variable, and the jacobian $J = \zeta[(1-x_B)|x_F|]^{-1}$ has been explicitely indicated [6]. The latter reduces to unity in the high-energy limit and it is therefore often omitted in the literature. The neutrino- and anti-neutrino-induced charged-current semi-inclusive cross sections read respectively

$$\frac{d^3\sigma^{\nu p\to \mu^- \Lambda X}}{dx_B dQ^2 d\zeta} = \frac{2\pi\alpha_{em}^2}{Q^4} J 8 \eta_W \Big[2(M_d^{\Lambda/p} + M_s^{\Lambda/p}) + 2(1-y)^2 M_{\bar{u}}^{\Lambda/p} \Big] , \tag{6}$$

and

$$\frac{d^3\sigma^{\bar{\nu} p\to \mu^+ \Lambda X}}{dx dQ^2 d\zeta} = \frac{2\pi\alpha_{em}^2}{Q^4} J 8 \eta_W \Big[2(M_{\bar{d}}^{\Lambda/p} + M_{\bar{s}}^{\Lambda/p}) + 2(1-y)^2 M_u^{\Lambda/p} \Big] , \tag{7}$$

where the dependencies of M_i appearing in eq. (6) and eq. (7) are to be understood as in eq. (5) and the factor η_W is defined in terms of the Fermi constant G_F, the W-boson mass M_W^2 and the electromagnetic coupling constant α_{em} as [7]

$$\eta_W = \frac{1}{2} \left(\frac{G_F M_W^2}{4\pi\alpha_{em}} \frac{Q^2}{Q^2 + M_W^2} \right)^2 . \tag{8}$$

As appropriate for a lowest-order calculation, we have assumed a vanishing longitudinal structure-function contribution in all formulas. We have further neglected charm quarks contributions.

In eqs. (5, 6, 7) the production of unpolarised Lambdas in the remnant direction is described by fracture functions $M_i^{\Lambda/p}(x, \zeta, Q^2)$ [2]. These distributions express the probability to find a parton of flavour i with fractional momentum x_B and virtuality Q^2 conditional to the detection of a Lambda with fraction ζ of the incoming proton energy. The scale dependence of fracture functions is given by the following evolution equations [2]

$$\begin{aligned} \frac{\partial}{\partial \log \mu^2} M_i^{\Lambda/p}\left(x_B, \zeta, \mu^2\right) &= \frac{\alpha_s(\mu^2)}{2\pi} \int_{x_B/(1-\zeta)}^1 \frac{du}{u} P_i^j(u) \, M_j^{\Lambda/p}\left(\frac{x_B}{u}, \zeta, \mu^2\right) \\ + \frac{\alpha_s(\mu^2)}{2\pi} \int_{x_B}^{x_B/(x_B+\zeta)} & \frac{du}{x_B(1-u)} \widehat{P}_i^{j,l}(u) \, f_{j/p}\left(\frac{x_B}{u}, \mu^2\right) \, D_l^\Lambda\left(\frac{\zeta u}{x_B(1-u)}, \mu^2\right) , \end{aligned} \tag{9}$$

where $P_i^j(u)$ and $\widehat{P}_i^{j,l}(u)$ are the regularised [8] and real [9] Altarelli-Parisi splitting functions, respectively. Eq. (9) describes both processes which contribute to Lambda production in the

Reaction type	Ref.	$\langle E_i \rangle$ (GeV)	$\langle W^2 \rangle$ (GeV^2)	$\langle Q^2 \rangle$ (GeV^2)	$\langle x_B \rangle$	Λ rates (%)
νp	[12]	50.0	-	-	-	7.0 ± 1.2
νn	[12]	50.0	-	-	-	7.0 ± 0.8
νp	[13]	42	34.7	8.7	0.2	5.2 ± 0.3
$\bar{\nu} p$	[13]	38.5	20.4	5.2	0.2	5.7 ± 0.4
μp	[14]	280	130	12	0.11	-
μD_2	[14]	280	130	12	0.11	-
μD_2	[15]	490	292	8.6	0.036	7.8 ± 1.6

Table 1: Data sets used in the present analysis. $\langle E_i \rangle$ is the average energy of the incoming lepton. Average kinematics and production rates for the various data set, when available, are indicated.

target-remnant direction. The homogeneous term on the right hand side of eq. (9) takes into account the effects of collinear parton radiation by the struck parton i while the Lambda originates from the fracture function itself. The inhomogeneous one instead takes into account the possibility that observed Lambda results from the fragmentation of the radiated parton l, emitted collinearly to the incoming parton j. This term in fact is a convolution of parton distributions $f_{j/p}(x_B, Q^2)$ and fragmentation functions $D_l^{\Lambda}(z, Q^2)$.

For the purpose of this paper, we use leading-order formulas both for semi-inclusive cross sections and for the fracture-function evolution equations. We note, however, that the full formalism is available at next-to-leading-order accuracy for both unpolarised [3] and polarised [10, 11] processes.

3 Data sets and Observables

The data used in the present analysis come from a variety of fixed-target experiments. We include neutrino and anti-neutrino DIS data which are crucial in providing minimal quark-flavour discrimination. In particular, stringent cuts ($x_B > 0.2$ and $W > 4$ GeV) in data from Ref. [12] enhance the contributions from the valence content of the nucleon; data from Ref. [13] are expected to be an admixture of valence and sea contributions and therefore constrain the relative normalisations of the various fracture functions. We further include in the fit neutral-current DIS data at higher beam energy presented in Refs. [14, 15] in order to provide the necessary information about the energy dependence of the cross sections.

Some care should be used in the selection of the targets. Since charged-current cross sections are significantly lower than neutral-current ones, many experiments have used nuclear targets. The first consequence is that nuclear corrections to fracture functions should be accounted for. Even more important for the purposes of this analysis, the fragmentation process itself might be affected by the nuclear medium, both in the current [16] and in the target [17] fragmentation region. In particular, it has been recently reported in Ref. [17] that strange-particle yields in neutrino-nuclei interactions are enhanced in the target region, probably due primary particles re-interaction with the nuclear medium. Since the particle yields show a mild power dependence

on the atomic number of the target, we include in the present analysis only proton- and deuteron-target data.

We would like to mention two effects which might affect the absolute normalisations of the various data sets. The first one is related to the definition of fracture functions. Many analyses quoted in Tab. (1) have estimated the contributions to the Lambda yield coming from the decay of higher-mass resonances. When not otherwise stated in the original publications, we interpret the published data as referring to an inclusive Lambda sample, that is the sum of promptly produced Lambdas and Lambdas coming from the decay of higher-mass resonances, corrected for unseen decay modes (a typical example is the $\Sigma^0 \to \Lambda\gamma$ decay mode discussed in Ref. [14]). The decay of higher-mass resonances infact happens at time scales much larger than the ones typical of perturbative processes and their effects will be effectively incorporated in fracture functions.

The second problem is posed by the contamination of Lambda yield by secondary Lambdas produced by the interaction of primary pions with detector material. This effect has been intensively studied in Ref. [18] and estimated to contribute up to 20% to the Lambda yield. It is unknown to us to which extent this correction has been properly estimated and applied to all data sets.

We close this Section discussing the choice and the reconstruction of the observable to be used in the fit. By definition, cross sections differential in the Lambda fractional energy are insensitive to the phase space region in which the latter has been produced. In this variable, the current- and target-fragmentation contributions overlap and the extraction of the latter therefore crucially depends on the precision with which we describe current fragmentation with available Lambda fragmentation functions. In order to overcome this problem, we consider differential cross sections in the Feynman variable x_F which offer, to lowest order, a kinematical separation of the two contributions. The use of such a variable is however not free from additional issues: Lambda-mass effects introduced via eq. (4) may be sizeable, as suggested by the values of the averaged hadronic final-state invariant mass $\langle W^2 \rangle$ quoted in Tab. (1). Such effects are however not compatible with the pQCD factorisation theorem. In the present analysis, Lambda-mass effects are therefore applied a posteriori to the Lambda leptoproduction cross sections σ^Λ, as described in Ref. [19]. The value in each x_F-bin is calculated as follows

$$\frac{1}{\sigma_{\rm DIS}}\frac{\Delta\sigma_i^\Lambda}{\Delta x_F^i} = \frac{1}{\sigma_{\rm DIS}}\frac{1}{\Delta x_F^i}\int dE_l \Phi(E_l) \int_\Omega dx_B dQ^2 \int_0^{1-x_B} d\zeta \frac{d^3\sigma^\Lambda(E_l)}{dx_B dQ^2 d\zeta}\,\Theta^i(x_F)\,, \qquad (10)$$

where the index i labels the i-th bin and the bin-size is specified by $\Delta x_F^i = x_F^{i+1} - x_F^i$, with x_F^i representing the experimental bin-edges. Mass corrections are enforced with the kinematical constraint $\Theta^i(x_F) = \theta(x_F - x_F^i)\,\theta(x_F^{i+1} - x_F)$, with x_F calculated via eq. (4). The label Ω stands for the set of cuts which define the DIS selection of a given analysis. The resulting differential cross sections are then normalised with respect to the inclusive DIS cross section

$$\sigma_{\rm DIS} = \int dE_l \Phi(E_l) \int_\Omega dx_B dQ^2 \frac{d^2\sigma^\Lambda(E_l)}{dx_B dQ^2}\,, \qquad (11)$$

calculated with parton-distribution functions of Ref. [20]. Both cross sections are integrated over the lepton flux factor $\Phi(E_l)$ expressed in units of GeV^{-1}. For monochromatic electron and muon

beams of energy $E_{l,0}$, the latter simply reduces to $\delta(E_l - E_{l,0})$. For neutrino and anti-neutrino beams we use the flux-factor parametrisations extracted by dedicated analyses [21]. We finally note that mass-corrected distributions are derived by using eq. (3) and eq. (4) and therefore in principle require the knowledge of the Lambda transverse momentum. From the very precise data of Ref. [18] we know that the Lambda p_t-spectrum is dominated by p_t values much smaller than its mass. We therefore approximate in eq. (4) the transverse mass m_T^2 with Lambda mass m_Λ^2 whose value is taken to be $m_\Lambda = 1115.683$ MeV [7].

4 Modelling Lambda Fracture Functions

The fracture formalism relies on the assumption that leading particle production in the target-fragmentation region is a leading-twist process. The latter has been strikingly confirmed by experimental observation of hard diffraction at HERA [22, 23]. In the present context, however, the limited amount of data is often presented as Q^2-integrated single-differential distributions, a fact which prevents any conclusion to be drawn. We only note that such hypothesis might be indirectly supported by the moderate value of the average Q^2 for the semi-inclusive reactions quoted in Tab. (1) and by the mild increase of the Lambda average multiplicity $\langle n(\Lambda)\rangle$ as a function Q^2, as seen in data [18].

Although the scale dependence of fracture functions is predicted by perturbative QCD, they still need to be modelled at some low scale and evolved to scales relevant to the experiments; the free parameters controlling their input distributions can then constrained by a fit to data. The input distributions are in general surfaces in the (x_B, ζ) space and contain a large number of free parameters needed to control the energy and flavour dependences of the cross sections. Since the hard scattering process occurs on time scales much shorter than spectator-fragmentation ones, we assume that, at an arbitrary low scale Q_0^2, fracture functions factorise into ordinary parton distributions $f_{i/p}(x_B, Q_0^2)$ and what we adress as spectator-fragmentation functions $\widetilde{D}_i^{\Lambda/p}(z)$

$$(1 - x_B)\, M_i^{\Lambda/p}\left(x_B, \zeta, Q_0^2\right) = M_i^{\Lambda/p}(x_B, z, Q_0^2) = f_{i/p}(x_B, Q_0^2)\widetilde{D}_i^{\Lambda/p}(z)\,,\ i = q, \bar{q}, g\,. \tag{12}$$

We take advantage of the sea-valence decomposition offered by the parton distributions of Ref. [20] to further decompose the valence parton contributions as

$$M_{q=u,d}^{\Lambda/p}(x_B, z, Q_0^2) = q_{val}(x_B, Q_0^2)\widetilde{D}_{q_{val}}^{\Lambda/p}(z) + q_{sea}(x_B, Q_0^2)\widetilde{D}_{q_{sea}}^{\Lambda/p}(z)\,. \tag{13}$$

For the non-perturbative spectator-fragmentation function we choose a simple functional form of the type

$$\widetilde{D}_i^{\Lambda/p}(z) = \overline{N_i} z^{\alpha_i}\,(1 - z)^{\beta_i}\,. \tag{14}$$

In order to minimise correlations between parameters, the normalisation coefficients in eq. (14) are defined as follows

$$\overline{N_i} = N_i\Big[\int_0^1 dz\, z^{\alpha_i}\,(1 - z)^{\beta_i}\Big]^{-1}, \quad \alpha_i, \beta_i > -1\,, \tag{15}$$

and N_i are used as free parameters in the fit.

The inclusion of deuteron-target data in the fit requires the knowledge of neutron-to-Lambda fracture functions. As a first approximation we assume u-d isospin symmetry

$$M_d^{\Lambda/n}(x_B, z, Q^2) = M_u^{\Lambda/p}(x_B, z, Q^2), \quad M_u^{\Lambda/n}(x_B, z, Q^2) = M_d^{\Lambda/p}(x_B, z, Q^2)\,. \tag{16}$$

Limiting ourselves to the discussion of the valence region and indicating in parenthesis the flavour structure of the spectator system, eq. (16) implies that

$$\widetilde{D}_{u(ud)}^{\Lambda/p} = \widetilde{D}_{d(ud)}^{\Lambda/n} \quad \text{and} \quad \widetilde{D}_{d(uu)}^{\Lambda/p} = \widetilde{D}_{u(dd)}^{\Lambda/n}. \tag{17}$$

The validity of these assumptions will be discussed in Section 6.

Given the input distributions in eqs. (12,13), set at an initial scale $Q_0^2 = 0.5$ GeV^2, we numerically solve the fracture-functions evolution equations in eq. (9) by using a finite-difference method in x_B-space in slices of ζ. We use the leading-order proton parton distribution of Ref. [20] and Λ fragmentation functions of Refs. [19] extracted taking into account target-hadron mass effects. For consitency, we follow the original evolution scheme of Ref. [20]. We evolve light-quarks fracture functions to leading-logarithmic accuracy by using a fixed flavour-number scheme. Heavy-quarks effects are included in the running of the strong coupling at the heavy-quark mass thresholds and $\Lambda_{\rm QCD}^{(n_f)}$ values are taken from Ref. [20].

As a final remark to this section we would like to discuss the impact of the inhomogeneous term in eq. (9) on the observables entering the fit. As a first step we have checked that, in the current region where the leading order semi-inclusive cross sections are proportional to the product of parton distributions and fragmentation functions, a reasonable description of μp data of Ref. [14] can be obtained both in shape and in normalisation by using parton distributions and fragmentation functions of Refs. [20] and Ref. [19], respectively. We then use fragmentation functions of Ref. [19] in the calculation of the inhomogenous term appering in eq. (9). At the observable level such term accumulates, as expected, at small $|x_F|$ as a result of the z shape of Lambda fragmentation functions. Moreover it contributes only at the percent level to the x_F distributions since it describes Lambda production from the fragmentation of radiated partons with transverse momentum greater than the minimum momentum transfer involved in the process, that is Q_0^2. As such it only contributes to the small radiative tail of the Lambda p_t-spectrum.

The radiative contributions generated by the inhomogeneous term and the universality issue of fragmentation functions could be studied in detail in processes that do not show any leading particle effect, for example the production of anti-Lambdas [14] or light mesons [24] off protons, or in target-like Lambda production in a perturbative regime (*i.e.* with sufficiently large transverse momentum, $p_t \geq 1$ GeV).

5 Fitting procedure

Each of the assumed Lambda spectator-fragmentation functions in eq. (14) contains three free parameters (one normalisation and two exponents). Our fitting strategy is the following: we first tentatively assume as many different fragmentation functions as possible types of struck partons (valence or sea u, valence or sea d, other sea quarks, gluon). The observable $1/\sigma_{\rm DIS}\, d\sigma^{\Lambda}/dx_F$ is then reconstructed via eq. (10) and the best fit parameter values are determined using `MINUIT` [25]

Reaction type	Ref.	partial χ^2	# fitted points
νp	[12]	4.77	5
νn	[12]	3.25	5
νp	[13]	6.36	8
$\bar{\nu} p$	[13]	9.08	8
μp	[14]	9.90	8
μD_2	[14]	10.58	9
μD_2	[15]	0.20	3

Table 2: Partial χ^2 contributions and number of points in the fit for each data set.

$\widetilde{D}_i^{\Lambda/p}$	N_i	α_i	β_i
u_{val}	0.046 ± 0.006	2.82 ± 1.19	0.39 ± 0.33
d_{val}	0.027 ± 0.006	$= \alpha_{u_{val}}$	1.28 ± 0.51
q_{sea}	0.078 ± 0.010	0	1.84 ± 0.63

Table 3: Best-fit values according to eq. (14).

program. We assume that the uncertainties on the cross sections combine statistical and systematic errors so that we use the simplest version of the χ^2-function as a merit function, although this neglects correlations between data points (the number of the latter is rather limited and amounts to 46). We then study the eigenvalues and the eigenvectors of the fit covariance matrix to identify any parameters that are badly constrained by the fit. We fix them by making some assumptions about their values and we repeat the fit with the remaining parameters.

With the available data, for example, the fit can not constrain distinct sea-quark fracture functions. We therefore assume a common spectator-fragmentation function for all of them, $\widetilde{D}_{q_{sea}}^{\Lambda/p}$. Moreover the fit is found to be insensitive to the choice of the gluon spectator fragmentation function. This is not unexpected since the gluon is coupled to electroweak probes only through higher orders. For this reason, we fix the gluon spectator-fragmentation functions to be equal to the sea one, $\widetilde{D}_g^{\Lambda/p} = \widetilde{D}_{q_{sea}}^{\Lambda/p}$, reducing the number of free parameters to nine. In such a fit the smallest eigenvalues of the Hessian matrix correspond to eigenvectors whose largest components are associated with the parameters α_i. The poor determination of such parameters can be partly associated to mass effects in the reconstruction of the observable in eq. (10) via eq. (4). The parameter $\alpha_{q_{sea}}$ is compatible with zero within errors so we fix it to this value. Furthermore, the parameters $\alpha_{u_{val}}$ and $\alpha_{d_{val}}$ are equal to each other within errors, so that we assume $\alpha_{u_{val}} = \alpha_{d_{val}}$, reducing the number of free parameters to seven. Fixing some of the parameters to a definite value is indeed an arbitrary procedure. We can motivate this choice only a posteriori by noting that, when these parameters are optimsed by the fit, the value of the χ^2 function is only marginally reduced. The best seven-parameter fit yields a $\chi^2/d.o.f. = 44.14/(46-7) = 1.13$. The partial χ^2 and the number of points included in the fit for each data set are displayed in Tab. (2). The results for the best-fit parameters are reported in Tab. (3) along with parameter errors as calculated by the `MINUIT` routine `HESSE`, which assumes a parabolic behaviour of the χ^2 function

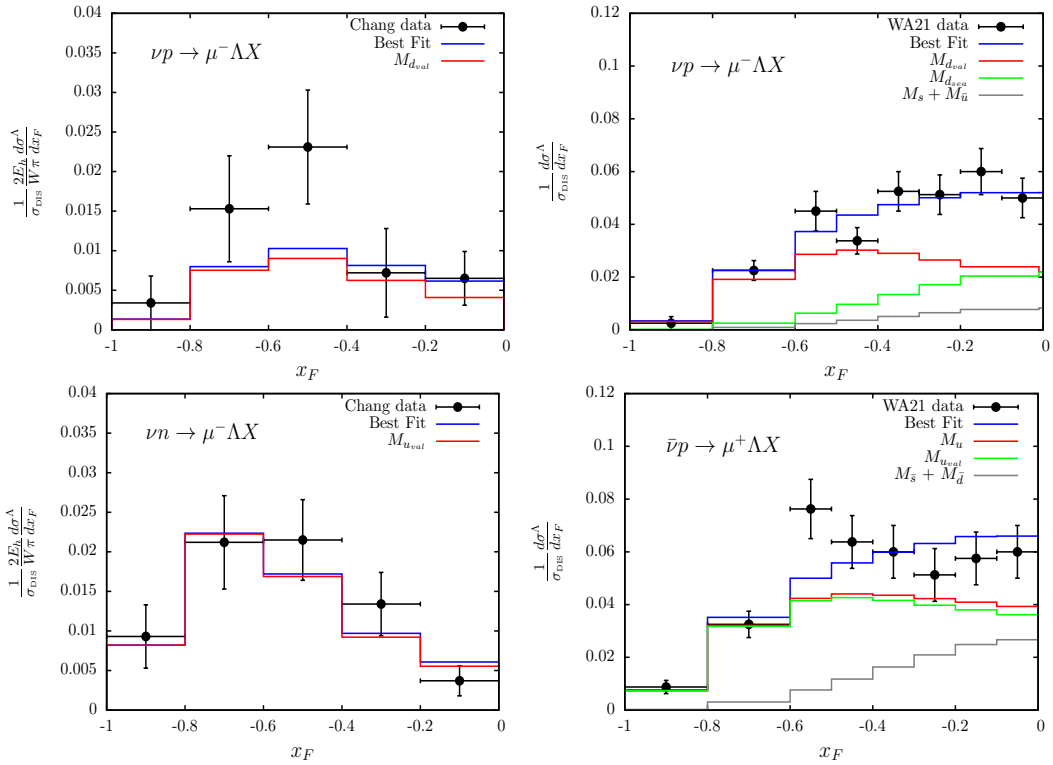

Figure 1: Best fit predictions compared to normalised x_F distributions for charged current semi-inclusive Lambda cross-sections from Ref. [12] (left panels) and Ref. [12] (right panels). Various quark-flavour proton-to-Lambda fracture functions contributions are shown. Note the additional factor $2E_h/(\pi\, W)$ which multiplies the normalised cross-sections from Ref. [12].

in parameter space around the minimum.

The best-determined parameters are the three normalisations, which implies that three independent distributions are in fact sufficient to handle the normalisation spread between the various data sets. The four parameters controlling the shape of the spectator functions have substantially larger uncertainties. The sources of the latter are primarily related to the intrinsic correlation between the α_i and β_i parameters introduced by the specific functional form assumed for the spectator functions in eq. (14). We also note that, at low centre-of-mass energy, where mass corrections introduced via eq. (4) are sizeable, a large portion of the x_F spectrum is controlled by the behaviour of the spectator functions in the neighbourhood of $z = 1$; the shape of the predicted spectrum is thus mainly determined by the β_i parameter alone. Therefore, parametrisations with more modulable behaviour at large z could improve the description of the x_F spectra. These improvements are probably marginal given the quality of the data used in this fit, but they might be necessary when dealing with higher quality data as presented, for example, in Ref. [18].

Given the stringent cut on the DIS selection, the data of Ref. [12] constrain the valence-quark fracture-function contributions, $M_{q_{val}}$, which in fact almost saturate the spectrum, as shown in the left column of Fig. (1). The first row of Fig. (1) reveals instead a normalisation tension between νp data from Ref. [13] and Ref. [12] which however can be tolerated in view of

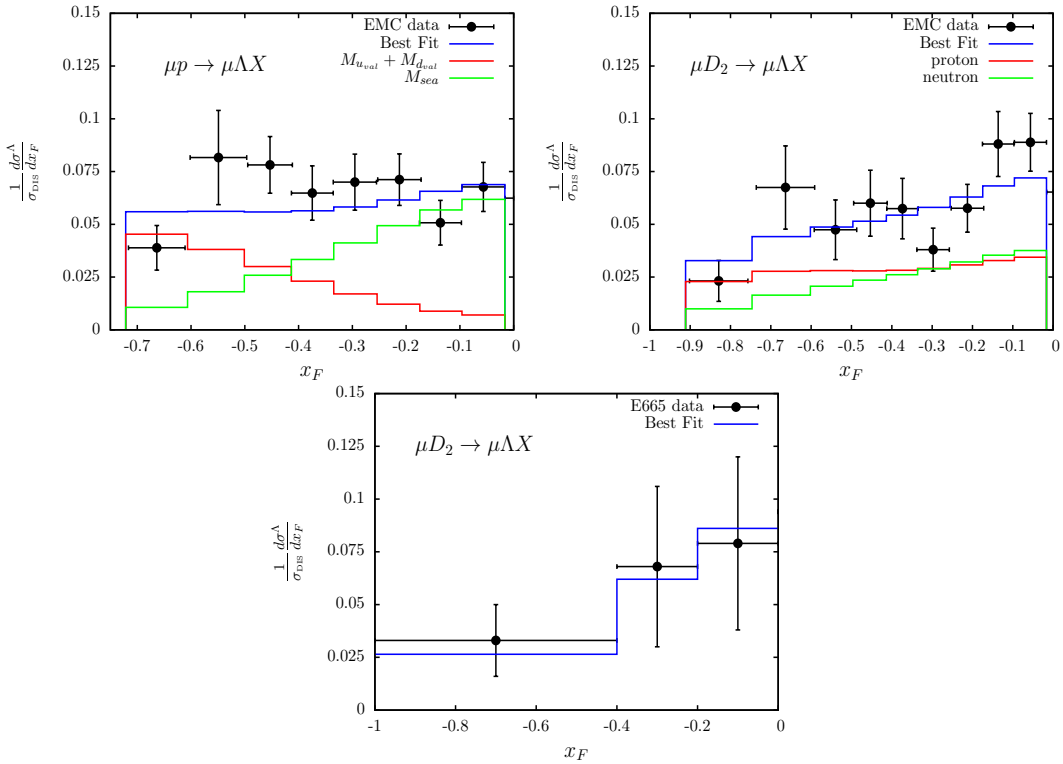

Figure 2: Best fit predictions compared to normalised x_F distributions for μp (left panel) and μD_2 (middle panel) data from Ref. [14] and μD_2 (right panel) data from Ref. [15]. In the μp case valence- and sea-quark fracture functions contributions are separately shown. In the μD_2 case the proton and neutron contributions are separately shown.

the partial χ^2 presented in Tab. (3). The second row shows a slight shape deformation in the predictions for νn data from Ref. [12] which is probably due to the normalisation constraint induced by $\bar{\nu} p$ data from Ref. [13] on the individual $M_{u_{val}}$ and $M_{q_{sea}}$ distributions. The fit indeed indicates, as expected from the valence-parton counting rules [1], that Lambdas are produced more abundantly and more forward by the fragmentation of ud-spectator system with respect to a uu- one.

We show in Fig. (2) the best-fit predictions for data from Ref. [14] and Ref. [15] for which the incident muon beam energy is significantly higher than neutrino and anti-neutrino ones. Quite interestingly, the spectrum at large $|x_F|$ is dominated by valence-quark fracture functions, as shown in the upper left panel of Fig. (3). The differences between $M_{u_{val}}$ and $M_{d_{val}}$ distributions is responsible for the different large $|x_F|$ behaviour on different targets, as shown in the upper right panel of Fig. (3). In all these plots, given the higher values of $\langle W^2 \rangle$ involved, Lambda-mass corrections play a less prominent role and therefore the z shape of the sea-quark fracture functions, as parametrised in Tab. (3), are clearly visible in these distributions. The results discussed above are stable against the variation of the arbitrary scale Q_0^2 at which fracture functions are factorised into parton distributions and spectator-fragmentation functions. The χ^2 function, in fact, shows a very mild dependence on Q_0^2 as the latter is varied below the measured range between 0.5 and 1.0 GeV^2.

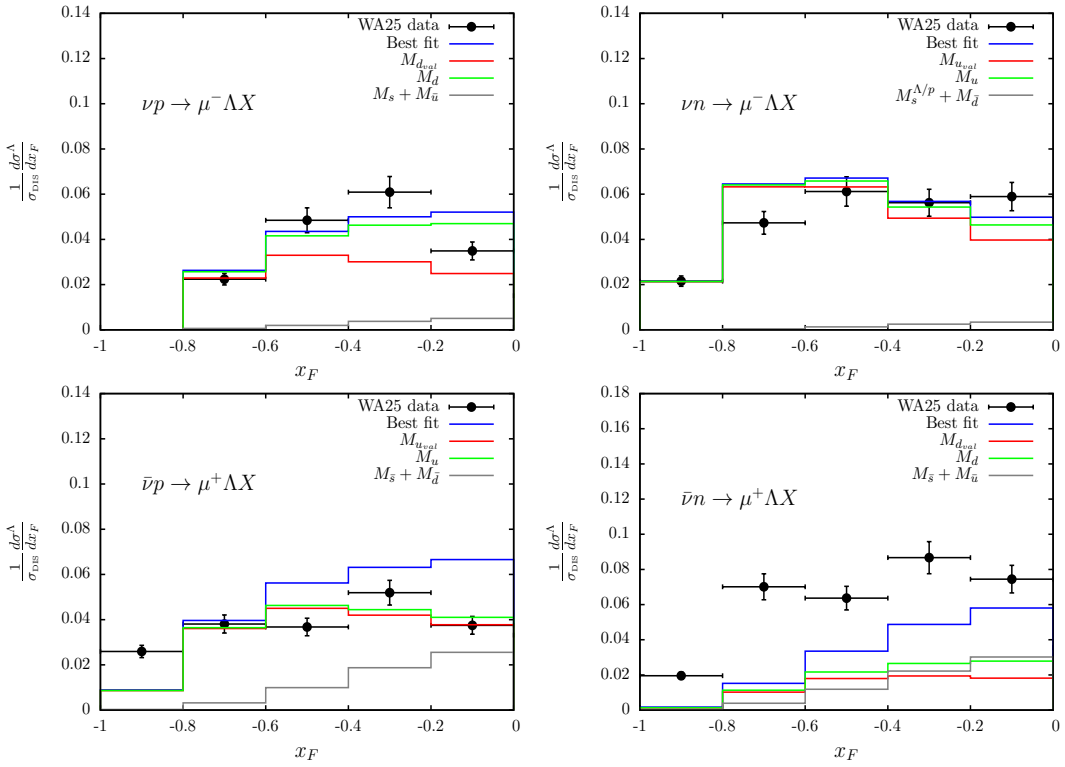

Figure 3: Best-fit predictions compared to normalised x_F-distributions for charged current semi-inclusive Lambda cross-sections from Refs. [26, 27]. Various quark-flavour proton-to-Lambda fracture functions contributions are shown.

6 Predictions

In this last section we wish to discuss the degree of predictivity of the model. It is of particular importance to determine to which extent the model is able to reproduce x_F distributions coming from data not included in the fit or observables other than the ones used in the fit. At the same time, the quality of the agreement with the data will pinpoint sectors of the model which may need to be improved.

The comparisons often require the reconstruction of the current fragmentation term, which is obtained with the semi-inclusive version of eqs. (6,7) where fracture functions are substituted by appropriate products of parton distributions and fragmentation functions. Such term has been estimated to leading order by using the parton distributions of Ref. [20] and the fragmentation functions of Ref. [19].

As a first example, we consider Lambda production in neutrino- and anti-neutrino-induced charged-current DIS on proton and neutron targets [26]. These data provide a full flavour discrimination of the spectator system and can be used to test the assumptions made in eq. (16). Unfortunately, the x_F distributions for these data are presented in Ref. [26] as histograms without errors. In a subsequent paper by the same collaboration [27], the Lambda yields are updated but no x_F distributions are shown.

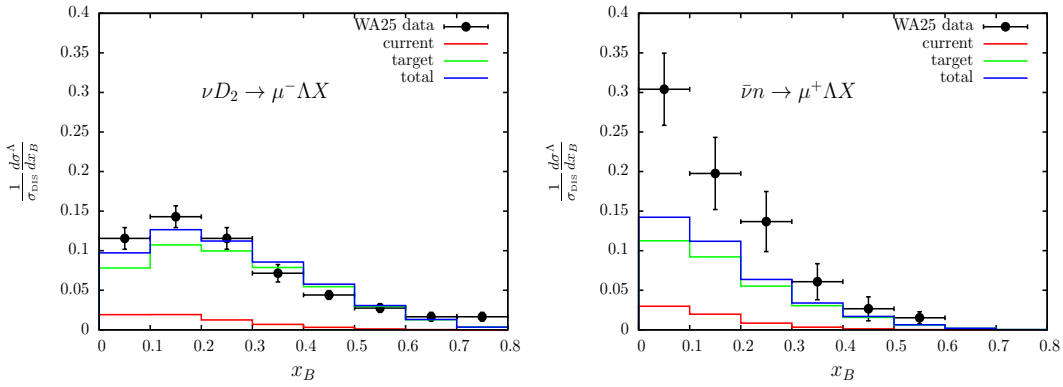

Figure 4: Normalised x_B distributions in νD_2 (left panel) and $\bar{\nu} n$ (right panel) scattering. Data are taken from Ref. [27].

In order to gauge the agreement of the best-fit model predictions with these data, we have assessed the errors in the following way. First the histograms from Ref. [26] have been scaled down to the updated yields of Ref. [27] assuming no change in their shape. Then we have assumed that the relative errors of the x_F distributions in each x_F bin are equal. This in turn implies that they are respectively equal to the relative error on the corresponding Lambda yield. This procedure guarantees that upon integration over x_F, the experimental yield and its error are correctly recovered.

The best-fit predictions are compared to data in Fig. (3). We note that, in general, the cross sections on proton target are fairly reproduced in normalisation, as expected, since the Lambda yields in $\bar{\nu}p$- and νp-scattering of Ref. [27] are in agreement within errors with those of data included in the fit [13, 12]. The distributions show however some stress in shape at low values of $|x_F|$. The shapes of the model predictions reflect those of the data used in the fit [13, 12], which are shown in the right-hand-side panels of Fig. (1). The comparison with neutron-target data reveals that, in this case, the model does not perform equally well. In particular, the νn cross sections seem to peak at too large values of $|x_F|$, a behaviour mainly driven by the νn data of Ref. [12] and illustrated in the lower left panel of Fig. (1). While all these distributions are quite well reproduced in normalisation, the model significantly underestimates the $\bar{\nu} n$-scattering data. The level of disagreement of data and theory might indicate that $\widetilde{D}^{\Lambda/p}_{d(uu)} < \widetilde{D}^{\Lambda/n}_{u(dd)}$, contrary to our assumptions in eq. (16). This interpretation is however subject to caution, as we discuss in the following.

The same data are presented in Fig. (4) in terms of normalised x_B distributions. We remind the reader that we integrate over the x_B variable in the reconstruction of the x_F distributions (eq. (10)). Therefore the comparison of the x_B distributions with the data constitutes a non-trivial test for the model. Excellent agreement is found for the νD_2 cross section, both in shape and in normalisation, as already seen for the $\bar{\nu}p$ and νp x_F distributions from the same data set and shown in the left-hand-side panels of Fig. (3). On the other hand, model predictions for the $\bar{\nu} n$ cross section fail to reproduce experimental distributions, as in the corresponding x_F distribution in the lower right panel of Fig. (3). Since the largest differences in the νD_2 and $\bar{\nu} n$

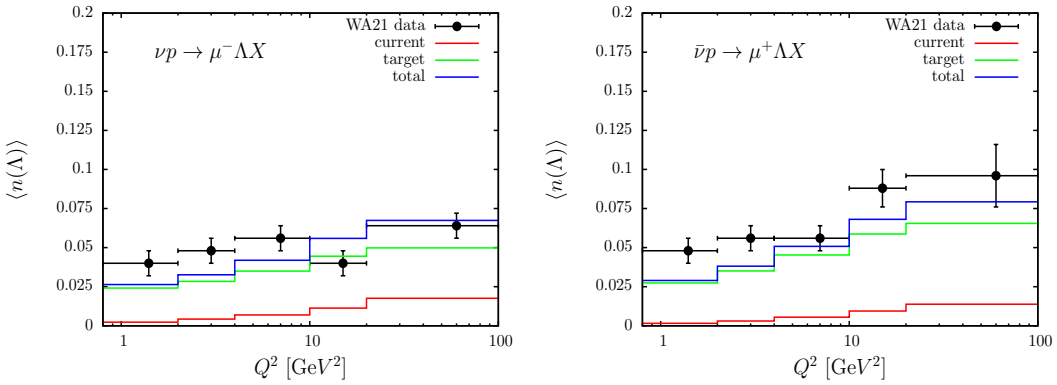

Figure 5: Lambda average multiplicity as a function of Q^2 in νp (left panel) and $\bar{\nu} p$ (right panel) scattering. Current and target contributions are separately shown. Data are from Ref. [13].

cross sections appear in the smallest x_B bin, there might exist some asymmetry in the sea-quark spectator functions which we instead assume to be all equal to each other.

It was originally suggested in Ref. [26] that target Lambdas are more abundantly produced by $\bar{\nu}\bar{s}$-scattering than in νs-scattering, based on the idea that $\bar{\nu}\bar{s}$-scattering leaves the correct hypercharge in the target spectator. Such a process would indeed enhance the yield at small x_B. In our framework, this hypothesis should be translated into an asymmetry of the spectator functions in the strange sector, $\widetilde{D}_{\bar{s}}^{\Lambda/p} > \widetilde{D}_{s}^{\Lambda/p}$. While a general asymmetry in the sea-quark spectator functions can be easily accomodated in the fit by increasing the number of free parameters, the cross sections used in the regression cannot separately constrain the parameters of $\widetilde{D}_{\bar{s}}^{\Lambda/p}$ and $\widetilde{D}_{s}^{\Lambda/p}$, because of the linear combinations of sea-quark fracture functions that enter the structure functions in eqs. (6,7).

In this respect, leptoproduction of target Lambdas in dimuon (anti-)neutrino-nucleon deep-inelastic scattering could represent an alternative sensitive test of the latter hypothesis. In this process, a (anti-)charm, produced by a charged current, semileptonically decays in the current-fragmentation region into a final-state, secondary, muon. Given the small off-diagonal quark-mixing CKM matrix elements, this process is able to probe directly the (anti-)strange component of the nucleon [28] and consequently the proposed Lambda asymmetry, $M_{\bar{s}}^{\Lambda/p} > M_{s}^{\Lambda/p}$, in the target-fragmentation region.

To conclude we show in Fig. (5) the model predictions for the averaged Lambda multiplicity as a function of Q^2 in νp and $\bar{\nu} p$ charged-current DIS cross sections. Although the x_F distributions from this data set [13] have been already used in the fit and therefore agreement in normalisation might be expected, the model is also able to reproduce reasonably well the observed Q^2 dependence, with a tendency to undershoot the data at the lowest value of Q^2. Since the Q^2 dependence built in the model via fracture-function evolution equations can be considered one of the most stringent predictions of the underlying theoretical framework, the reasonable agreement between data and predictions can be considered the first step towards a conclusive validation of the perturbative framework. The validation procedure and the model itself would, in fact, highly benefit from the constraints imposed by multi-differential distrubutions. Cross

sections at fixed x_B and x_F as a function of Q^2, for example, could give access, through scaling violations, to the presently unconstrained gluon fracture function, $M_g^{\Lambda/p}(x_B, z, Q^2)$.

7 Summary and conclusions

In this paper we have analysed experimental data on the production of Lambda hyperons in the SIDIS target-fragmentation region in terms of fracture functions. A model for the latter has been proposed and the free parameters appearing in the input distributions have been fixed by performing a fit to a variety of neutral- and charged-current semi-inclusive DIS cross sections. The main features seen in the data can be fairly reproduced by the model. In particular the spectator-fragmentation functions associated with the removal of valence quarks populate the very forward part of the x_F-spectrum at large and negative values of x_F. On the other hand, the sea-quark contribution is concentrated at small and negative values of x_F. The predictions based on the model are in fair agreement with data not included in the fit and with observables depending on variables which are integrated over in the analysis, especially the Q^2 dependence of the Lambda multiplicity, which is a stringent test of the underlying theoretical framework. Although further tests and additional experimental informations are necessary to validate and eventually improve the model, it may be used to quantitatively investigate spectator-fragmentation mechanisms within a perturbative QCD approach. Since higher-order calculations are available in the literature, the analysis can be extended to next-to-leading order accuracy. The model can be easily generalised to take into account Lambda polarisation allowing spin-transfer studies [29] in the target region and it may find application in the estimation of nuclear corrections to target fragmentation.

Acknowledgements

We gratefully acknowledge M. Stratmann and S. Albino for providing us with their fragmentation-function routines. We especially acknowledge D. Naumov for interesting discussions related to backgrounds in Lambda production in DIS and for providing us the neutrino flux parametrisations. We wish to thank the organizers of the Workshop "Strangeness polarization in semi-inclusive and exclusive Lambda production" held in ECT*, Trento, in October 2008 and all the participants for stimulating discussions on this topic. We finally thank Laurent Favart, Dmitry Naumov, Jean-René Cudell and Luca Trentadue for a critical reading of the manuscript prior to submission.

References

[1] M. Basile *et al.*, *Nuovo Cim.* **A66** (1981) 129.

[2] L. Trentadue and G. Veneziano, *Phys. Lett.* **B323** (1994) 201.

[3] D. Graudenz, *Nucl. Phys.* **B432** (1994) 351.

[4] J. C. Collins, *Phys. Rev.* **D57** (1998) 3051.

[5] M. Grazzini, L. Trentadue and G. Veneziano, *Nucl. Phys.* **B519** (1998) 394.

[6] J. Levelt and P. J. Mulders, *Phys. Rev.* **D49** (1994) 96.

[7] J. Beringer *et al.* (Particle Data Group), *Phys. Rev.* **D86** (2012) 010001.

[8] G. Altarelli and G. Parisi, *Nucl. Phys.* **B126** (1977) 298.

[9] E. Konishi, A. Ukawa and G. Veneziano, *Nucl. Phys.* **B157** (1979) 45.

[10] D. de Florian, C. A. Garcia Canal and R. Sassot, *Nucl. Phys.* **B470** (1996) 195.

[11] D. de Florian and R. Sassot, *Nucl. Phys.* **B488** (1997) 367.

[12] C. C. Chang *et al.*, *Phys. Rev.* **D27** (1983) 2776.

[13] G. T. Jones *et al.* (WA21 Collaboration), *Z. Phys.* **C57** (1993) 197.

[14] M. Arneodo *et al.* (EMC Collaboration), *Z. Phys.* **C34** (1987) 283.

[15] M. R. Adams *et al.* (E665 Collaboration), *Z. Phys.* **C61** (1994) 539.

[16] A. Airapetian *et al.* (Hermes Collaboration), *Eur. Phys. J.* **A47** (2011) 113.

[17] N. M. Agababyan *et al.* (SKAT Collaboration), *Phys. Atom. Nucl.* **70** (2007) 1731.

[18] P. Astier *et al.* (NOMAD Collaboration), *Nucl. Phys.* **B621** (2002) 3.

[19] S. Albino, B. A. Kniehl and G. Kramer, *Nucl. Phys.* **B803** (2008) 42.

[20] M. Glück, E. Reya and A. Vogt, *Z. Phys.* **C67** (1995) 433.

[21] P. Astier *et al.* (NOMAD Collaboration), *Nucl. Instrum. Meth.* **A515** (2003) 800.

[22] M. Derrick *et al.* (ZEUS Collaboration), *Phys. Lett.* **B315** (1993) 481.

[23] T. Ahmed *et al.* (H1 Collaboration), *Nucl. Phys.* **B429** (1994) 477.

[24] M. Osipenko *et al.* (CLAS Collaboration), *Phys. Rev.* **D80** (2009) 032004.

[25] F. James and M. Roos, *Comput. Phys. Commun.* **10** (1975) 343.

[26] D. Allasia *et al.* (WA25 Collaboration), *Nucl. Phys.* **B224** (1983) 1.

[27] D. Allasia *et al.* (WA25 Collaboration), *Phys. Lett.* **B154** (1983) 231.

[28] S. Alekhin, S. Kulagin and R. petti, *Phys. Lett.* **B675** (2009) 433.

[29] J. R. Ellis *et al.*, *Eur. Phys. J.* **C52** (2007) 283.